

Measurements of WW and WZ Production in W + jets Final States in $p\bar{p}$ Collisions

- V. M. Abazov,³⁴ B. Abbott,⁷² B. S. Acharya,²⁸ M. Adams,⁴⁸ T. Adams,⁴⁶ G. D. Alexeev,³⁴ G. Alkhazov,³⁸ A. Alton,^{60,*} G. Alverson,⁵⁹ G. A. Alves,² M. Aoki,⁴⁷ A. Askew,⁴⁶ B. Åsman,⁴⁰ S. Atkins,⁵⁷ O. Atramentov,⁶⁴ K. Augsten,⁹ C. Avila,⁷ J. BackusMayes,⁷⁹ F. Badaud,¹² L. Bagby,⁴⁷ B. Baldin,⁴⁷ D. V. Bandurin,⁴⁶ S. Banerjee,²⁸ E. Barberis,⁵⁹ P. Baringer,⁵⁵ J. Barreto,³ J. F. Bartlett,⁴⁷ U. Bassler,¹⁷ V. Bazterra,⁴⁸ A. Bean,⁵⁵ M. Begalli,³ C. Belanger-Champagne,⁴⁰ L. Bellantoni,⁴⁷ S. B. Beri,²⁶ G. Bernardi,¹⁶ R. Bernhard,²¹ I. Bertram,⁴¹ M. Besançon,¹⁷ R. Beuselinck,⁴² V. A. Bezzubov,³⁷ P. C. Bhat,⁴⁷ V. Bhatnagar,²⁶ G. Blazey,⁴⁹ S. Blessing,⁴⁶ K. Bloom,⁶³ A. Boehlein,⁴⁷ D. Boline,⁶⁹ E. E. Boos,³⁶ G. Borissov,⁴¹ T. Bose,⁵⁸ A. Brandt,⁷⁵ O. Brandt,²² R. Brock,⁶¹ G. Brooijmans,⁶⁷ A. Bross,⁴⁷ D. Brown,¹⁶ J. Brown,¹⁶ X. B. Bu,⁴⁷ M. Buehler,⁴⁷ V. Buescher,²³ V. Bunichev,³⁶ S. Burdin,^{41,†} T. H. Burnett,⁷⁹ C. P. Buszello,⁴⁰ B. Calpas,¹⁴ E. Camacho-Pérez,³¹ M. A. Carrasco-Lizarraga,⁵⁵ B. C. K. Casey,⁴⁷ H. Castilla-Valdez,³¹ S. Chakrabarti,⁶⁹ D. Chakraborty,⁴⁹ K. M. Chan,⁵³ A. Chandra,⁷⁷ E. Chapon,¹⁷ G. Chen,⁵⁵ S. Chevalier-Théry,¹⁷ D. K. Cho,⁷⁴ S. W. Cho,³⁰ S. Choi,³⁰ B. Choudhary,²⁷ S. Cihangir,⁴⁷ D. Claes,⁶³ J. Clutter,⁵⁵ M. Cooke,⁴⁷ W. E. Cooper,⁴⁷ M. Corcoran,⁷⁷ F. Couderc,¹⁷ M.-C. Cousinou,¹⁴ A. Croc,¹⁷ D. Cutts,⁷⁴ A. Das,⁴⁴ G. Davies,⁴² K. De,⁷⁵ S. J. de Jong,³³ E. De La Cruz-Burelo,³¹ F. Déliot,¹⁷ R. Demina,⁶⁸ D. Denisov,⁴⁷ S. P. Denisov,³⁷ S. Desai,⁴⁷ C. Deterre,¹⁷ K. DeVaughan,⁶³ H. T. Diehl,⁴⁷ M. Diesburg,⁴⁷ P. F. Ding,⁴³ A. Dominguez,⁶³ T. Dorland,⁷⁹ A. Dubey,²⁷ L. V. Dudko,³⁶ D. Duggan,⁶⁴ A. Duperrin,¹⁴ S. Dutt,²⁶ A. Dyshkant,⁴⁹ M. Eads,⁶³ D. Edmunds,⁶¹ J. Ellison,⁴⁵ V. D. Elvira,⁴⁷ Y. Enari,¹⁶ H. Evans,⁵¹ A. Evdokimov,⁷⁰ V. N. Evdokimov,³⁷ G. Facini,⁵⁹ T. Ferbel,⁶⁸ F. Fiedler,²³ F. Filthaut,³³ W. Fisher,⁶¹ H. E. Fisk,⁴⁷ M. Fortner,⁴⁹ H. Fox,⁴¹ S. Fuess,⁴⁷ A. Garcia-Bellido,⁶⁸ G. A. García-Guerra,^{31,‡} V. Gavrilov,³⁵ P. Gay,¹² W. Geng,^{14,61} D. Gerbaudo,⁶⁵ C. E. Gerber,⁴⁸ Y. Gershtein,⁶⁴ G. Ginther,^{47,68} G. Golovanov,³⁴ A. Goussiou,⁷⁹ P. D. Grannis,⁶⁹ S. Greder,¹⁸ H. Greenlee,⁴⁷ Z. D. Greenwood,⁵⁷ E. M. Gregores,⁴ G. Grenier,¹⁹ Ph. Gris,¹² J.-F. Grivaz,¹⁵ A. Grohsjean,¹⁷ S. Grünendahl,⁴⁷ M. W. Grünewald,²⁹ T. Guillemin,¹⁵ G. Gutierrez,⁴⁷ P. Gutierrez,⁷² A. Haas,^{67,§} S. Hagopian,⁴⁶ J. Haley,⁵⁹ L. Han,⁶ K. Harder,⁴³ A. Harel,⁶⁸ J. M. Hauptman,⁵⁴ J. Hays,⁴² T. Head,⁴³ T. Hebbeker,²⁰ D. Hedin,⁴⁹ H. Hegab,⁷³ A. P. Heinson,⁴⁵ U. Heintz,⁷⁴ C. Hensel,²² I. Heredia-De La Cruz,³¹ K. Herner,⁶⁰ G. Hesketh,^{43,||} M. D. Hildreth,⁵³ R. Hirosky,⁷⁸ T. Hoang,⁴⁶ J. D. Hobbs,⁶⁹ B. Hoeneisen,¹¹ M. Hohlfeld,²³ Z. Hubacek,^{9,17} V. Hynek,⁹ I. Iashvili,⁶⁶ Y. Ilchenko,⁷⁶ R. Illingworth,⁴⁷ A. S. Ito,⁴⁷ S. Jabeen,⁷⁴ M. Jaffré,¹⁵ D. Jamin,¹⁴ A. Jayasinghe,⁷² R. Jesik,⁴² K. Johns,⁴⁴ M. Johnson,⁴⁷ A. Jonckheere,⁴⁷ P. Jonsson,⁴² J. Joshi,²⁶ A. W. Jung,⁴⁷ A. Juste,³⁹ K. Kaadze,⁵⁶ E. Kajfasz,¹⁴ D. Karmanov,³⁶ P. A. Kasper,⁴⁷ I. Katsanos,⁶³ R. Kehoe,⁷⁶ S. Kermiche,¹⁴ N. Khalatyan,⁴⁷ A. Khanov,⁷³ A. Kharchilava,⁶⁶ Y. N. Kharzeev,³⁴ J. M. Kohli,²⁶ A. V. Kozelov,³⁷ J. Kraus,⁶¹ S. Kulikov,³⁷ A. Kumar,⁶⁶ A. Kupco,¹⁰ T. Kurča,¹⁹ V. A. Kuzmin,³⁶ J. Kvita,⁸ S. Lammers,⁵¹ G. Landsberg,⁷⁴ P. Lebrun,¹⁹ H. S. Lee,³⁰ S. W. Lee,⁵⁴ W. M. Lee,⁴⁷ J. Lellouch,¹⁶ L. Li,⁴⁵ Q. Z. Li,⁴⁷ S. M. Lietti,⁵ J. K. Lim,³⁰ D. Lincoln,⁴⁷ J. Linnemann,⁶¹ V. V. Lipaev,³⁷ R. Lipton,⁴⁷ Y. Liu,⁶ A. Lobodenko,³⁸ M. Lokajicek,¹⁰ R. Lopes de Sa,⁶⁹ H. J. Lubatti,⁷⁹ R. Luna-Garcia,^{31,¶} A. L. Lyon,⁴⁷ A. K. A. Maciel,² D. Mackin,⁷⁷ R. Madar,¹⁷ R. Magaña-Villalba,³¹ S. Malik,⁶³ V. L. Malyshev,³⁴ Y. Maravin,⁵⁶ J. Martínez-Ortega,³¹ R. McCarthy,⁶⁹ C. L. McGivern,⁵⁵ M. M. Meijer,³³ A. Melnitchouk,⁶² D. Menezes,⁴⁹ P. G. Mercadante,⁴ M. Merkin,³⁶ A. Meyer,²⁰ J. Meyer,²² F. Miconi,¹⁸ N. K. Mondal,²⁸ G. S. Muanza,¹⁴ M. Mulhearn,⁷⁸ E. Nagy,¹⁴ M. Naimuddin,²⁷ M. Narain,⁷⁴ R. Nayyar,²⁷ H. A. Neal,⁶⁰ J. P. Negret,⁷ P. Neustroev,³⁸ S. F. Novaes,⁵ T. Nunnemann,²⁴ G. Obrant,^{38,‡‡} J. Orduna,⁷⁷ N. Osman,¹⁴ J. Osta,⁵³ G. J. Otero y Garzón,¹ M. Padilla,⁴⁵ A. Pal,⁷⁵ N. Parashar,⁵² V. Parihar,⁷⁴ S. K. Park,³⁰ R. Partridge,^{74,§} N. Parua,⁵¹ A. Patwa,⁷⁰ B. Penning,⁴⁷ M. Perfilov,³⁶ Y. Peters,⁴³ K. Petridis,⁴³ G. Petrillo,⁶⁸ P. Pétroff,¹⁵ R. Piegaia,¹ M.-A. Pleier,⁷⁰ P. L. M. Podesta-Lerma,^{31,***} V. M. Podstavkov,⁴⁷ P. Polozov,³⁵ A. V. Popov,³⁷ M. Prewitt,⁷⁷ D. Price,⁵¹ N. Prokopenko,³⁷ J. Qian,⁶⁰ A. Quadt,²² B. Quinn,⁶² M. S. Rangel,² K. Ranjan,²⁷ P. N. Ratoff,⁴¹ I. Razumov,³⁷ P. Renkel,⁷⁶ M. Rijssenbeek,⁶⁹ I. Ripp-Baudot,¹⁸ F. Rizatdinova,⁷³ M. Rominsky,⁴⁷ A. Ross,⁴¹ C. Royon,¹⁷ P. Rubinov,⁴⁷ R. Ruchti,⁵³ G. Safronov,³⁵ G. Sajot,¹³ P. Salcido,⁴⁹ A. Sánchez-Hernández,³¹ M. P. Sanders,²⁴ B. Sanghi,⁴⁷ A. S. Santos,⁵ G. Savage,⁴⁷ L. Sawyer,⁵⁷ T. Scanlon,⁴² R. D. Schamberger,⁶⁹ Y. Scheglov,³⁸ H. Schellman,⁵⁰ T. Schliephake,²⁵ S. Schlobohm,⁷⁹ C. Schwanenberger,⁴³ R. Schwienhorst,⁶¹ J. Sekaric,⁵⁵ H. Severini,⁷² E. Shabalina,²² V. Shary,¹⁷ A. A. Shchukin,³⁷ R. K. Shivpuri,²⁷ V. Simak,⁹ V. Sirotenko,⁴⁷ P. Skubic,⁷² P. Slattery,⁶⁸ D. Smirnov,⁵³ K. J. Smith,⁶⁶ G. R. Snow,⁶³ J. Snow,⁷¹ S. Snyder,⁷⁰ S. Söldner-Rembold,⁴³ L. Sonnenschein,²⁰ K. Soustruznik,⁸ J. Stark,¹³ V. Stolin,³⁵ D. A. Stoyanova,³⁷ M. Strauss,⁷² D. Strom,⁴⁸ L. Stutte,⁴⁷ L. Suter,⁴³ P. Svoisky,⁷² M. Takahashi,⁴³ A. Tanasijczuk,¹ M. Titov,¹⁷ V. V. Tokmenin,³⁴ Y.-T. Tsai,⁶⁸ K. Tschann-Grimm,⁶⁹ D. Tsybychev,⁶⁹ B. Tuchming,¹⁷ C. Tully,⁶⁵ L. Uvarov,³⁸ S. Uvarov,³⁸ S. Uzunyan,⁴⁹ R. Van Kooten,⁵¹ W. M. van Leeuwen,³² N. Varelas,⁴⁸ E. W. Varnes,⁴⁴ I. A. Vasilyev,³⁷ P. Verdier,¹⁹ L. S. Vertogradov,³⁴ M. Verzocchi,⁴⁷ M. Vesterinen,⁴³ D. Vilanova,¹⁷ P. Vokac,⁹ H. D. Wahl,⁴⁶

M. H. L. S. Wang,⁴⁷ J. Warchol,⁵³ G. Watts,⁷⁹ M. Wayne,⁵³ M. Weber,^{47,††} L. Welty-Rieger,⁵⁰ A. White,⁷⁵ D. Wicke,²⁵
 M. R. J. Williams,⁴¹ G. W. Wilson,⁵⁵ M. Wobisch,⁵⁷ D. R. Wood,⁵⁹ T. R. Wyatt,⁴³ Y. Xie,⁴⁷ R. Yamada,⁴⁷ W.-C. Yang,⁴³
 T. Yasuda,⁴⁷ Y. A. Yatsunenko,³⁴ Z. Ye,⁴⁷ H. Yin,⁴⁷ K. Yip,⁷⁰ S. W. Youn,⁴⁷ J. Yu,⁷⁵ T. Zhao,⁷⁹ B. Zhou,⁶⁰ J. Zhu,⁶⁰
 M. Zielinski,⁶⁸ D. Ziemińska,⁵¹ and L. Zivkovic⁷⁴

(D0 Collaboration)

¹Universidad de Buenos Aires, Buenos Aires, Argentina

²LAFEX, Centro Brasileiro de Pesquisas Físicas, Rio de Janeiro, Brazil

³Universidade do Estado do Rio de Janeiro, Rio de Janeiro, Brazil

⁴Universidade Federal do ABC, Santo André, Brazil

⁵Instituto de Física Teórica, Universidade Estadual Paulista, São Paulo, Brazil

⁶University of Science and Technology of China, Hefei, People's Republic of China

⁷Universidad de los Andes, Bogotá, Colombia

⁸Charles University, Faculty of Mathematics and Physics, Center for Particle Physics, Prague, Czech Republic

⁹Czech Technical University in Prague, Prague, Czech Republic

¹⁰Center for Particle Physics, Institute of Physics, Academy of Sciences of the Czech Republic, Prague, Czech Republic

¹¹Universidad San Francisco de Quito, Quito, Ecuador

¹²LPC, Université Blaise Pascal, CNRS/IN2P3, Clermont, France

¹³LPSC, Université Joseph Fourier Grenoble 1, CNRS/IN2P3, Institut National Polytechnique de Grenoble, Grenoble, France

¹⁴CPPM, Aix-Marseille Université, CNRS/IN2P3, Marseille, France

¹⁵LAL, Université Paris-Sud, CNRS/IN2P3, Orsay, France

¹⁶LPNHE, Universités Paris VI and VII, CNRS/IN2P3, Paris, France

¹⁷CEA, Irfu, SPP, Saclay, France

¹⁸IPHC, Université de Strasbourg, CNRS/IN2P3, Strasbourg, France

¹⁹IPNL, Université Lyon 1, CNRS/IN2P3, Villeurbanne, France and Université de Lyon, Lyon, France

²⁰III. Physikalisches Institut A, RWTH Aachen University, Aachen, Germany

²¹Physikalisches Institut, Universität Freiburg, Freiburg, Germany

²²II. Physikalisches Institut, Georg-August-Universität Göttingen, Göttingen, Germany

²³Institut für Physik, Universität Mainz, Mainz, Germany

²⁴Ludwig-Maximilians-Universität München, München, Germany

²⁵Fachbereich Physik, Bergische Universität Wuppertal, Wuppertal, Germany

²⁶Panjab University, Chandigarh, India

²⁷Delhi University, Delhi, India

²⁸Tata Institute of Fundamental Research, Mumbai, India

²⁹University College Dublin, Dublin, Ireland

³⁰Korea Detector Laboratory, Korea University, Seoul, Korea

³¹CINVESTAV, Mexico City, Mexico

³²Nikhef, Science Park, Amsterdam, The Netherlands

³³Radboud University Nijmegen, Nijmegen, The Netherlands and Nikhef, Science Park, Amsterdam, The Netherlands

³⁴Joint Institute for Nuclear Research, Dubna, Russia

³⁵Institute for Theoretical and Experimental Physics, Moscow, Russia

³⁶Moscow State University, Moscow, Russia

³⁷Institute for High Energy Physics, Protvino, Russia

³⁸Petersburg Nuclear Physics Institute, St. Petersburg, Russia

³⁹Institució Catalana de Recerca i Estudis Avançats (ICREA), and Institut de Física d'Altes Energies (IFAE), Barcelona, Spain

⁴⁰Stockholm University, Stockholm and Uppsala University, Uppsala, Sweden

⁴¹Lancaster University, Lancaster LA1 4YB, United Kingdom

⁴²Imperial College London, London SW7 2AZ, United Kingdom

⁴³The University of Manchester, Manchester M13 9PL, United Kingdom

⁴⁴University of Arizona, Tucson, Arizona 85721, USA

⁴⁵University of California Riverside, Riverside, California 92521, USA

⁴⁶Florida State University, Tallahassee, Florida 32306, USA

⁴⁷Fermi National Accelerator Laboratory, Batavia, Illinois 60510, USA

⁴⁸University of Illinois at Chicago, Chicago, Illinois 60607, USA

⁴⁹Northern Illinois University, DeKalb, Illinois 60115, USA

⁵⁰Northwestern University, Evanston, Illinois 60208, USA

⁵¹Indiana University, Bloomington, Indiana 47405, USA

⁵²Purdue University Calumet, Hammond, Indiana 46323, USA

- ⁵³*University of Notre Dame, Notre Dame, Indiana 46556, USA*
⁵⁴*Iowa State University, Ames, Iowa 50011, USA*
⁵⁵*University of Kansas, Lawrence, Kansas 66045, USA*
⁵⁶*Kansas State University, Manhattan, Kansas 66506, USA*
⁵⁷*Louisiana Tech University, Ruston, Louisiana 71272, USA*
⁵⁸*Boston University, Boston, Massachusetts 02215, USA*
⁵⁹*Northeastern University, Boston, Massachusetts 02115, USA*
⁶⁰*University of Michigan, Ann Arbor, Michigan 48109, USA*
⁶¹*Michigan State University, East Lansing, Michigan 48824, USA*
⁶²*University of Mississippi, University, Mississippi 38677, USA*
⁶³*University of Nebraska, Lincoln, Nebraska 68588, USA*
⁶⁴*Rutgers University, Piscataway, New Jersey 08855, USA*
⁶⁵*Princeton University, Princeton, New Jersey 08544, USA*
⁶⁶*State University of New York, Buffalo, New York 14260, USA*
⁶⁷*Columbia University, New York, New York 10027, USA*
⁶⁸*University of Rochester, Rochester, New York 14627, USA*
⁶⁹*State University of New York, Stony Brook, New York 11794, USA*
⁷⁰*Brookhaven National Laboratory, Upton, New York 11973, USA*
⁷¹*Langston University, Langston, Oklahoma 73050, USA*
⁷²*University of Oklahoma, Norman, Oklahoma 73019, USA*
⁷³*Oklahoma State University, Stillwater, Oklahoma 74078, USA*
⁷⁴*Brown University, Providence, Rhode Island 02912, USA*
⁷⁵*University of Texas, Arlington, Texas 76019, USA*
⁷⁶*Southern Methodist University, Dallas, Texas 75275, USA*
⁷⁷*Rice University, Houston, Texas 77005, USA*
⁷⁸*University of Virginia, Charlottesville, Virginia 22901, USA*
⁷⁹*University of Washington, Seattle, Washington 98195, USA*

(Received 1 December 2011; published 2 May 2012)

We study WW and WZ production with $\ell\nu qq$ ($\ell = e, \mu$) final states using data collected by the D0 detector at the Fermilab Tevatron Collider corresponding to 4.3 fb^{-1} of integrated luminosity from $p\bar{p}$ collisions at $\sqrt{s} = 1.96 \text{ TeV}$. Assuming the ratio between the production cross sections $\sigma(WW)$ and $\sigma(WZ)$ as predicted by the standard model, we measure the total WV ($V = W, Z$) cross section to be $\sigma(WV) = 19.6^{+3.2}_{-3.0} \text{ pb}$ and reject the background-only hypothesis at a level of 7.9 standard deviations. We also use b -jet discrimination to separate the WZ component from the dominant WW component. Simultaneously fitting WW and WZ contributions, we measure $\sigma(WW) = 15.9^{+3.7}_{-3.2} \text{ pb}$ and $\sigma(WZ) = 3.3^{+4.1}_{-3.3} \text{ pb}$, which is consistent with the standard model predictions.

DOI: 10.1103/PhysRevLett.108.181803

PACS numbers: 14.70.Fm, 13.85.Ni, 13.85.Qk, 14.70.Hp

The study of the production of VV ($V = W, Z$) boson pairs provides an important test of the electroweak sector of the standard model (SM). In $p\bar{p}$ collisions at $\sqrt{s} = 1.96 \text{ TeV}$, the next-to-leading order (NLO) SM cross sections for these processes are $\sigma(WW) = 11.7 \pm 0.8 \text{ pb}$, $\sigma(WZ) = 3.5 \pm 0.3 \text{ pb}$, and $\sigma(ZZ) = 1.4 \pm 0.1 \text{ pb}$ [1]. Measuring a significant departure in cross section or deviations in the predicted kinematic distributions would indicate the presence of anomalous gauge boson couplings [2] or new particles in extensions of the SM [3]. This analysis also provides a proving ground for the advanced analysis techniques used in low mass Higgs boson searches [4]. The production of VV in $p\bar{p}$ collisions at the Fermilab Tevatron Collider has been observed in fully leptonic decay modes [5] and, more recently, in leptons + jets decay modes [6], where the combined $WW + WZ$ cross section was measured. In

$p\bar{p}$ collisions at $\sqrt{s} = 7 \text{ TeV}$ at the LHC, diboson production has been studied by using the fully leptonic decay modes [7].

In this Letter, we report observation of the associated production of a W boson that decays leptonically and a second vector boson that decays hadronically ($WV \rightarrow \ell\nu qq$; $\ell = e^\pm$ or μ^\pm , and ν and q denote matter or antimatter as appropriate). The data used for this analysis correspond to 4.3 fb^{-1} of integrated luminosity collected between 2006 and 2009 by the D0 detector [8] at the Fermilab Tevatron Collider. The D0 detector dijet mass resolution for W/Z decays of $\approx 18\%$ results in significant overlap of $W \rightarrow qq$ and $Z \rightarrow qq$ dijet mass peaks. Therefore, we first consider WW and WZ simultaneously and measure the total WV cross section assuming the ratio of WW to WZ cross sections as predicted by the SM. We then apply b -jet identification to separate

the WZ contribution, where the Z boson decays into $b\bar{b}$ pairs, from the dominant WW production.

Candidate events in the electron channel are required to satisfy a single electron trigger or a trigger requiring electrons and jets, which results in a combined trigger efficiency of $(98^{+2}_{-3})\%$ for the $e\nu qq$ event selection described below. A comprehensive suite of triggers in the muon channel, based on leptons, jets, and their combination, achieves a trigger efficiency of $(95 \pm 5)\%$ for the $\mu\nu qq$ event selection.

To select $WV \rightarrow \ell\nu qq$ candidates, we require a single reconstructed electron (muon) with transverse momentum $p_T > 15$ GeV (20 GeV) and pseudorapidity $|\eta| < 1.1$ (2.0) [9], missing transverse energy $\cancel{E}_T > 20$ GeV, and two or three jets reconstructed by using a cone algorithm [10]. The jets must have $p_T > 20$ GeV, $|\eta| < 2.5$, and at least two tracks within the jet cone [10] originating from the $p\bar{p}$ interaction vertex. Lepton candidates must be spatially matched to a track that originates from the primary $p\bar{p}$ interaction vertex, and they must be isolated from energy depositions in the calorimeter and other tracks in the central tracking detector. To reduce background from processes that do not contain $W \rightarrow \ell\nu$, we require that the W transverse mass [11] is $M_T^{\ell\nu}(\text{GeV}) > 40 - 0.5\cancel{E}_T$. In addition, we restrict $M_T^{\mu\nu} < 200$ GeV to suppress muon candidates with poorly measured momenta.

Signal and most of the background processes are modeled with Monte Carlo (MC) simulation. The signal events are generated with PYTHIA [12] using CTEQ6L1 parton distribution functions (PDFs) [13] and include all SM decays. The fixed-order matrix element generator ALPGEN [14] with CTEQ6L1 PDF is used to generate $W + \text{jets}$, $Z + \text{jets}$, and $t\bar{t}$ events. The fixed-order matrix element generator COMPHEP [15] is used to produce single top-quark MC samples with CTEQ6M PDF [13]. Both ALPGEN and COMPHEP are interfaced to PYTHIA for parton showering and hadronization. The MC events undergo a GEANT-based [16] detector simulation and are reconstructed by using the same algorithms as used for D0 data. The effect of multiple $p\bar{p}$ interactions is included by overlaying data events from random beam crossings on simulated events. The next-to-NLO (NNLO) cross section is used to normalize the $Z + \text{jets}$ (light and heavy-flavor jets) [17]. The approximate NNLO cross section [18] is used to normalize the $t\bar{t}$ samples, while the single top-quark MC samples are normalized to the approximate next-to-NNLO cross section [19]. The normalization of the $W + \text{jets}$ MC sample (for all flavor contributions) is determined from the data. Additional NLO heavy-flavor corrections are calculated with MCFM [20] and applied to $Z/W + \text{heavy-flavor jets}$ MC samples.

The multijet background in which a jet is misidentified as a prompt lepton is determined from the data. For the muon channel, the multijet background is modeled with the data that fail the muon isolation requirements but pass all

other selections. For the electron channel, the multijet background is estimated by using a data sample containing events that pass less restrictive electron quality requirements. Both multijet samples are corrected for contributions from processes modeled by MC calculations. The multijet normalizations are determined from fits to the $M_T^{\ell\nu}$ distributions and assigned uncertainties of 20%.

To identify heavy quark (b and c) jets, in particular, those originating from Z decays, we use the D0 neural network (NN) b -tagging algorithm [21]. The NN is trained to separate light-flavor jets from heavy-flavor jets based on a combination of variables sensitive to the presence of tracks and vertices displaced from the primary $p\bar{p}$ interaction vertex. The NN outputs for the two highest p_T jets are then used as inputs to the final multivariate discriminant. We define nonoverlapping 0-, 1-, and 2-tag subchannels based on whether neither, only one, or both of the two highest p_T jets pass the least restrictive NN operating point, for which the b -jet identification efficiency and the light-flavor jet misidentification rate are approximately 80% and 10%, respectively. Scale factors are applied to the MC events to account for any difference in efficiency or misidentification rate between the data and simulation.

The dominant background is $W + \text{jets}$, and therefore the modeling of this process in ALPGEN and the corresponding sources of uncertainties were studied in detail. Comparison of ALPGEN with other generators [22] and with the data shows discrepancies in jet η , dijet angular separation, and the transverse momentum of the W boson candidate. Thus, the data are used to correct these quantities in the ALPGEN $W + \text{jets}$ and $Z + \text{jets}$ samples before b tagging is performed [23]. The possible bias in this procedure from the presence of the diboson signal in the data is small but is taken into account as a systematic uncertainty.

As the diboson events are generated with a LO generator, changes to the event kinematics and the acceptance due to a NLO and resummation effects are studied by using events from the MC@NLO [24] interfaced to HERWIG [25] for parton showering and hadronization and by using the CTEQ6M PDF set. Comparing kinematics at the generator level after final state radiation, we parameterize a two-dimensional correction matrix in the p_T of the diboson system and of the highest p_T boson. After applying this correction to our PYTHIA sample, we find good agreement with MC@NLO for all distributions studied. Half of the difference between the PYTHIA and MC@NLO predictions is used as a systematic uncertainty on the diboson production model, accounting for the possible effects of higher order corrections beyond NLO and of different showering scenarios.

The signal and the backgrounds are further separated by using a multivariate classifier to combine information from several variables. This analysis uses a random forest (RF) classifier [26,27], from which the output distribution is used as a final variable to measure the production cross

TABLE I. Number of events for the signal and each background after the combined fit of WV using the RF output distribution (with total uncertainties determined from the fit) and the number of events observed in the data.

	Electron channel	Muon channel
Diboson signal	1725 ± 84	1465 ± 67
$W/Z +$ light-flavor jets	$37\,232 \pm 1033$	$33\,516 \pm 709$
$W/Z +$ heavy-flavor jets	5371 ± 608	4854 ± 490
$t\bar{t}$ and single top	1746 ± 127	1214 ± 86
Multijet	$10\,630 \pm 1007$	1982 ± 384
Total predicted	$56\,704 \pm 635$	$43\,031 \pm 531$
Data	56 698	43 044

sections by performing a template fit. Fifteen well-modeled variables [28] that demonstrate a difference in probability density between the signal and at least one of the backgrounds are used as inputs to the RF. Among these variables, the invariant mass of the jet pair provides most of the discrimination between the signal and background. The RF is trained by using a fraction of each MC sample. The remainder of each MC sample, along with the multijet background samples, is then evaluated by the RF and used in the measurement.

Depending on the source, we consider the effect of systematic uncertainty on the normalization and/or on the shape of differential distributions for signal and backgrounds [28]. Systematic effects on the differential distributions of the ALPGEN $W +$ jets and $Z +$ jets MC events from changes of the renormalization and factorization scales and of the parameters used in the Mangano parton-jet matching algorithm [29] are also considered. Uncertainties on PDFs [30], as well as uncertainties from object reconstruction and identification, are evaluated for all MC samples.

The total WV cross section is determined from a fit to the data of the signal and background RF output distributions. The fit is performed simultaneously on the six distributions corresponding to the electron and muon channels and the 0-, 1-, and 2-tag subchannels. The fit is performed by minimizing a Poisson χ^2 function with respect to Gaussian priors on each of the systematic uncertainties [31]. The effects on separate samples or subchannels due to the same uncertainty are assumed to be 100% correlated. However, different uncertainties are assumed to be mutually independent. The total posterior uncertainty from the fit, including off-diagonal covariance terms, is reported in Table I. This posterior uncertainty is smaller than the prior uncertainty due to the significant constraint of the data in the region of low RF output, which contains very little expected diboson signal.

The fit simultaneously varies the signal and $W +$ jets contributions, thereby also determining the normalization factor for the $W +$ jets MC sample. This obviates the need for using the predicted ALPGEN cross section and provides a

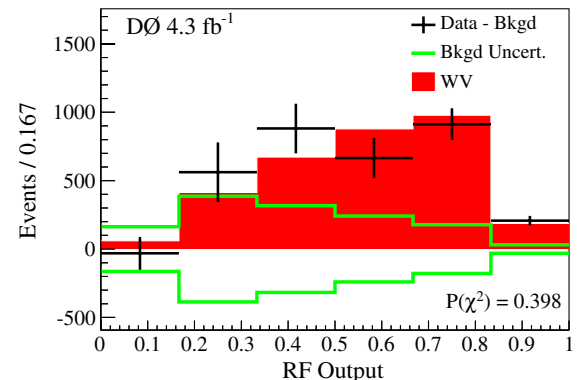


FIG. 1 (color online). A comparison of the measured WV signal (filled histogram) to background-subtracted data (points) in the RF output distribution (summed over electron and muon channels and 0-, 1-, and 2-tag subchannels), after the combined fit to data using the RF output distributions. Also shown is the posterior uncertainty (± 1 s.d.) on the subtracted background prediction. The χ^2 fit probability $P(\chi^2)$ is based on the residuals using data and MC statistical uncertainties.

more rigorous approach that incorporates an unbiased uncertainty from $W +$ jets when extracting the signal cross section. The $W +$ jets normalization factor from the fit is consistent with the theoretical NNLO prediction [32]. The yields for the signal and each background are given in Table I. Though the total diboson yield includes a small contribution from $ZZ \rightarrow \ell\ell qq$ events (1.5%), in which one of the charged leptons escapes detection, the cross sections presented here are corrected for this contribution assuming that the ratios between WW , WZ , and ZZ cross sections are given by the SM.

The fit of the total WV cross section using the RF output distributions yields $\sigma(WV) = 19.6^{+3.2}_{-3.0}$ pb, corresponding to an observed (expected) significance of 7.9 (5.9) standard deviations (s.d.). Figure 1 shows the background-subtracted RF output distribution summed over all subchannels after

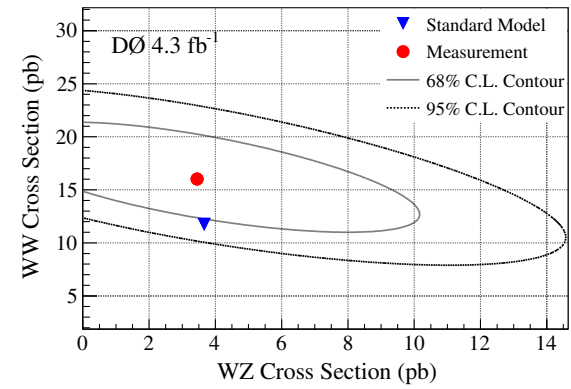


FIG. 2 (color online). Results from the simultaneous fit of $\sigma(WW)$ and $\sigma(WZ)$ using the RF output distributions. The plot shows the best fit value with 68% and 95% confidence level (C.L.) regions and the NLO SM prediction.

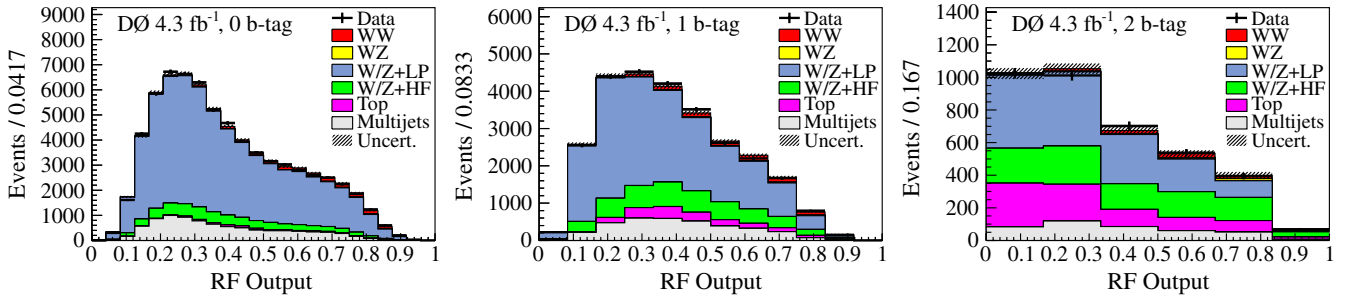


FIG. 3 (color online). A comparison of the signal + background prediction to the data in the RF output distribution (summed over electron and muon channels) for 0-, 1-, and 2-tag subchannels after the combined fit to data using the RF output distribution (LP denotes light partons such as u , d , s , or gluon, and HF denotes heavy flavor such as $c\bar{c}$ or $b\bar{b}$). The systematic uncertainty band is evaluated after the fit of the total WV cross section in the RF output distribution.

the fit. As a cross-check, we perform the measurement using the dijet mass distributions in place of the full RF output distributions [28]. This measurement yields a WV cross section of $\sigma(WV) = 18.3^{+3.8}_{-3.6}$ pb, consistent with that obtained by using the RF output distribution.

The fit is then performed with the signal divided into the separate WW and WZ components, which are allowed to float independently. The result of this simultaneous fit of $\sigma(WW)$ and $\sigma(WZ)$ using the RF output distributions is shown in Fig. 2. It yields $\sigma(WW) = 15.9^{+1.9}_{-1.5}(\text{stat})^{+3.2}_{-2.9} \times (\text{syst})$ pb and $\sigma(WZ) = 3.3^{+3.4}_{-2.7}(\text{stat})^{+2.2}_{-1.8}(\text{syst})$ pb. The RF output distributions for the 0-, 1-, and 2-tag subchannels from this fit are shown in Fig. 3. This measurement is also verified by fitting the dijet mass distribution, which yields $\sigma(WW) = 13.3^{+2.8}_{-2.2}(\text{stat})^{+3.6}_{-2.9}(\text{syst})$ pb and $\sigma(WZ) = 5.4^{+2.7}_{-2.6}(\text{stat})^{+4.5}_{-4.3}(\text{syst})$ pb. Figure 4 shows plots for the background-subtracted dijet mass after the dijet mass fit.

We also perform a fit in which we constrain the WW cross section to its SM prediction with a Gaussian prior equal to the theoretical uncertainty of 7% [1]. The fit of the RF output distribution yields a WZ cross section of $\sigma(WZ) = 6.5 \pm 0.9(\text{stat}) \pm 3.0(\text{syst})$ pb with an observed (expected) significance of 2.2 (1.2) s.d., and the dijet mass fit yields $\sigma(WZ) = 6.7 \pm 1.0(\text{stat}) \pm 3.9(\text{syst})$ pb with an observed (expected) significance of 1.7 (0.9) s.d. As

expected, now that $\sigma(WW)$ is constrained to the SM prediction, the fit requires a higher rate for WZ in order to account for the excess of signal-like events.

In summary, we have measured the cross section for total WV production to be $\sigma(WV) = 19.6^{+3.2}_{-3.0}$ pb ($V = W$ or Z) with a significance of 7.9 s.d. above the background-only hypothesis. This result demonstrates the ability of the D0 experiment to measure a dijet signal in a background-dominated final state directly relevant to low mass Higgs boson searches. Furthermore, we have used b -jet tagging to measure the contributions from WW and WZ and measured the cross sections for the separate processes to be $\sigma(WW) = 15.9^{+3.7}_{-3.2}$ pb and $\sigma(WZ) = 3.3^{+4.1}_{-3.3}$ pb. Although we cannot yet claim 3 s.d. evidence of a WZ signal in the $\ell\nu jj$ final states, the extracted WV and WZ cross sections are in agreement with the SM prediction, and their precise measurement represents an independent test to new physics which could manifest itself differently in different final states.

We thank the staffs at Fermilab and collaborating institutions and acknowledge support from the DOE and NSF (USA); CEA and CNRS/IN2P3 (France); FASI, Rosatom, and RFBR (Russia); CNPq, FAPERJ, FAPESP, and FUNDUNESP (Brazil); DAE and DST (India); Colciencias (Colombia); CONACyT (Mexico); KRF and

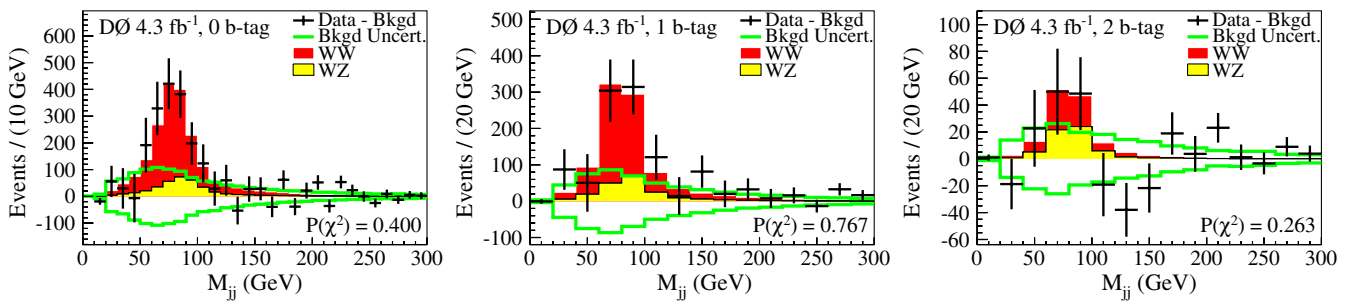


FIG. 4 (color online). A comparison of the measured WW and WZ signals (filled histograms) to background-subtracted data (points) in the dijet mass distribution (summed over electron and muon channels) for 0-, 1-, and 2-tag subchannels after the combined fit to data using the dijet mass distribution. Also shown is the posterior uncertainty (± 1 s.d.) on the subtracted background prediction. The χ^2 fit probability $P(\chi^2)$ is based on the residuals using data and MC statistical uncertainties.

KOSEF (Korea); CONICET and UBACyT (Argentina); FOM (The Netherlands); STFC and the Royal Society (United Kingdom); MSMT and GACR (Czech Republic); CRC Program and NSERC (Canada); BMBF and DFG (Germany); SFI (Ireland); The Swedish Research Council (Sweden); and CAS and CNSF (China).

*Visitor from Augustana College, Sioux Falls, SD, USA.

[†]Visitor from The University of Liverpool, Liverpool, United Kingdom.

[‡]Visitor from UPIITA-IPN, Mexico City, Mexico.

[§]Visitor from SLAC, Menlo Park, CA, USA.

^{||}Visitor from University College London, London, United Kingdom.

[¶]Visitor from Centro de Investigacion en Computacion-IPN, Mexico City, Mexico.

^{**}Visitor from ECFM, Universidad Autonoma de Sinaloa, Culiacán, Mexico.

^{††}Visitor from Universität Bern, Bern, Switzerland.

^{##}Deceased.

- [1] J. M. Campbell and R. K. Ellis, *Phys. Rev. D* **60**, 113006 (1999). We use MCFM version 6.0.
- [2] K. Hagiwara, S. Ishihara, R. Szalapski, and D. Zeppenfeld, *Phys. Rev. D* **48**, 2182 (1993).
- [3] J. C. Pati and A. Salam, *Phys. Rev. D* **10**, 275 (1974); **11**, 703(E) (1975); G. Altarelli, B. Mele, and M. Ruiz-Altaba, *Z. Phys. C* **45**, 109 (1989); **47**, 676(E) (1990); H. Davoudiasl, J. L. Hewett, and T. G. Rizzo, *Phys. Rev. D* **63**, 075004 (2001); H.-J. He, Y.-P. Kuang, Y.-H. Qi, B. Zhang, A. Belyaev, R. S. Chivukula, N. D. Christensen, A. Pukhov, and E. H. Simmons, *Phys. Rev. D* **78**, 031701 (2008).
- [4] V. M. Abazov *et al.* (D0 Collaboration), *Phys. Rev. Lett.* **104**, 071801 (2010); **105**, 251801 (2010); *Phys. Lett. B* **698**, 6 (2011).
- [5] T. Aaltonen *et al.* (CDF Collaboration), *Phys. Rev. Lett.* **104**, 201801 (2010); V. M. Abazov *et al.* (D0 Collaboration), *Phys. Lett. B* **695**, 67 (2011); *Phys. Rev. D* **84**, 011103 (2011).
- [6] T. Aaltonen *et al.* (CDF Collaboration), *Phys. Rev. Lett.* **103**, 091803 (2009); **104**, 101801 (2010).
- [7] S. Chairchyan *et al.* (CMS Collaboration), *Phys. Lett. B* **699**, 25 (2011); G. Aad *et al.* (ATLAS Collaboration), *Phys. Rev. Lett.* **107**, 041802 (2011); *Phys. Lett. B* **709**, 341 (2012); *Phys. Rev. Lett.* **108**, 041804 (2012).
- [8] B. Abbott *et al.* (D0 Collaboration), *Nucl. Instrum. Methods Phys. Res., Sect. A* **565**, 463 (2006); M. Abolins *et al.*, *Nucl. Instrum. Methods Phys. Res., Sect. A* **584**, 75 (2008); R. Angstadt *et al.*, *Nucl. Instrum. Methods Phys. Res., Sect. A* **622**, 298 (2010).
- [9] D0 uses a spherical coordinate system with the z axis running along the proton beam axis. The angles θ and ϕ are the polar and azimuthal angles, respectively. Pseudorapidity is defined as $\eta = -\ln[\tan(\theta/2)]$, in

which θ is measured with respect to the proton beam direction.

- [10] G. C. Blazey *et al.*, arXiv:hep-ex/0005012. The seeded cone algorithm with radius $\Delta\mathcal{R} = \sqrt{(\Delta\eta)^2 + (\Delta\phi)^2} = 0.5$ is used.
- [11] J. Smith, W. L. van Neerven, and J. A. M. Vermaseren, *Phys. Rev. Lett.* **50**, 1738 (1983).
- [12] T. Sjöstrand, S. Mrenna, and P. Skands, *J. High Energy Phys.* **05** (2006) 026. Version 6.409 is used.
- [13] J. Pumplin, D. R. Stump, J. Huston, H.-L. Lai, P. Nadolsky, and W.-K. Tung, *J. High Energy Phys.* **07** (2002) 012; D. Stump, J. Huston, J. Pumplin, W.-K. Tung, H. L. Lai, S. Kuhlmann, and J. F. Owens, *J. High Energy Phys.* **10** (2003) 046.
- [14] M. L. Mangano, F. Piccinini, A. D. Polosa, M. Moretti, and R. Pittau, *J. High Energy Phys.* **07** (2003) 001. Version 2.11 is used with the $W + c$ fix from v2.12.
- [15] E. Boos, V. Bunichev, M. Dubinin, L. Dudko, V. Edneral, V. Ilyin, A. Kryukov, V. Savrin, A. Semenov, and A. Sherstnev (CompHEP Collaboration), *Nucl. Instrum. Methods Phys. Res., Sect. A* **534**, 250 (2004).
- [16] R. Brun and F. Carminati, CERN Program Library Long Writeup No. W5013, 1993.
- [17] R. Gavin, Y. Li, F. Petriello, and S. Quackenbush, *Comput. Phys. Commun.* **182**, 2388 (2011).
- [18] N. Kidonakis and R. Vogt, *Phys. Rev. D* **78**, 074005 (2008).
- [19] N. Kidonakis, *Phys. Rev. D* **74**, 114012 (2006).
- [20] J. M. Campbell and R. K. Ellis, *Phys. Rev. D* **65**, 113007 (2002).
- [21] V. M. Abazov *et al.* (D0 Collaboration), *Nucl. Instrum. Methods Phys. Res., Sect. A* **620**, 490 (2010).
- [22] J. Alwall *et al.*, *Eur. Phys. J. C* **53**, 473 (2008).
- [23] V. M. Abazov *et al.* (D0 Collaboration), *Phys. Rev. Lett.* **107**, 011804 (2011).
- [24] S. Frixione and B. R. Webber, *J. High Energy Phys.* **06** (2002) 029; S. Frixione, P. Nason, and B. R. Webber, *J. High Energy Phys.* **08** (2003) 007. Version 3.3 is used.
- [25] G. Corcella, I. G. Knowles, G. Marchesini, S. Moretti, K. Odagiri, P. Richardson, M. H. Seymour, and B. R. Webber, *J. High Energy Phys.* **01** (2001) 010.
- [26] L. Breiman, *Mach. Learn.* **45**, 5 (2001).
- [27] I. Narsky, arXiv:physics/0507143.
- [28] See Supplemental Material at <http://link.aps.org/supplemental/10.1103/PhysRevLett.108.181803> for additional figures and information from the measurements of WW and WZ production in $W +$ jets final states at the D0 experiment at Fermilab Tevatron Collider such as modeling of input variables to the multivariate analysis, systematic uncertainties, and statistical significance of the signal yield.
- [29] S. Höche *et al.*, arXiv:hep-ph/0602031.
- [30] J. Pumplin, D. Stump, R. Brock, D. Casey, J. Huston, J. Kalk, H. L. Lai, and W. K. Tung, *Phys. Rev. D* **65**, 014013 (2001).
- [31] W. Fisher, Report No. FERMILAB-TM-2386-E, 2006.
- [32] R. Hamberg, W. L. van Neerven, and T. Matsuura, *Nucl. Phys.* **B359**, 343 (1991); **B644**, 403 (2002).